Properties of Er_2O_3 nanoparticles synthesized by a modified co-precipitation method

J. Castañeda-Contreras[a,*], V.F. Marañón-Ruiz[a], M.A. Meneses-Nava[b], H. Pérez- Ladrón de Guevara[a], R.A. Rodríguez Rojas[a], R. Chiu-Zárate[a]

[a] *Universidad de Guadalajara, Centro Universitario de los Lagos, Av. Enrique Díaz de León, S/N. Lagos de Moreno, Jalisco. 47460, México.*

[*] *Tel/fax: +52 1 474 742 3678.*

e-mail: jcc050769@yahoo.com.mx

[b] *Centro de Investigaciones en Óptica, A.C. Apartado Postal 1-948, León, Gto. México.*

Received 28 October 2014; accepted 19 January 2014

Er_2O_3 nanoparticles were synthesized by co-precipitation with the addition of ascorbate as stabilizing agent. The nanoparticles had spherical shapes with a mean diameter of 32 nm and were allocated in clusters, as determined by XRD, AFM, and optical microscopy. Characteristic green and red emissions from Er^{3+} were recorded by pumping the nanoparticles at 525 nm, 805 nm, and 975 nm. However, the luminescence spectra show an enhancement of red emission for NIR pump wavelengths. We proposed this behavior was due to phonon-assisted depopulation mechanisms and energy transfer processes related to the different excitation schemes.

Keywords: Erbium nanoparticles; optical materials and properties; spectroscopy.

PACS: 78.60.Lc; 78.67.Bf

1. Introduction

Currently, optical properties of lanthanide ions such as Er^{3+} are of great interest in optoelectronics technology [1-8]. In addition, erbium ions are particularly suitable for fluorescence and up-conversion of infrared to visible light because of a favorable electronic level scheme with equally spaced, long-lived excited states [9]. The fabrication of erbium-doped materials usually involves vacuum technologies such as ion implantation [10], epitaxy [11] and vapor deposition [12]. A low cost strategy is the direct addition of erbium-doped nanoparticles to solid hosts [13-15]. The co-precipitation method allows the synthesis of Er_2O_3 nanoparticles by the addition of coordinating ligands such as citrate [16] or poly-ethylene glycol [17]. The interaction between the ligands and lanthanide ions results in a positive charge that prevents aggregation of the species in solution [18]. This method allows the fabrication of water-soluble nanoparticles such as LaF_3:Er [19]. On the present study, we substituted the citrate with ascorbate by use of a new method to prepare Er_2O_3 nanoparticles. Spectroscopic studies were performed, such as absorption and luminescence spectra of the Er_2O_3. The structure and the corresponding energies of the recorded luminescence are reported and compared with these reported on the literature.

2. Material and methods

2.1. Synthesis of Er_2O_3 nanoparticles

The chemicals were of analytical grade, purchased from Sigma-Aldrich Co. and were utilized as received without any further treatment. The Er_2O_3 nanoparticles were synthesized by co-precipitation [20], with NaF as precipitator in presence of ascorbate ions in aqueous solution. The reaction began by dissolving 0.5 g of ascorbic acid and 0.0315 g of NaF in 10 ml of distilled water. The pH of the solution was adjusted to a value of 4 by adding some droplets of an aqueous solution of ammonium hydroxide (NH_4OH, 35 wt %). The resulting solution was heated at 70°C during 20 minutes. Subsequently, a solution of 1.25 g of erbium nitrate ($Er(NO_3)_3 \cdot 6H_2O$) dissolved in 2 ml of ethanol (ETOH) was added to the NaF-ascorbic acid solution. The resulting mixture was left under continuous stirring for two hours at room temperature. The nanoparticles were collected by centrifugation at 3000 rpm, washed twice and dried at room temperature under vacuum. Finally, the samples were heated at 800°C in air for three hours.

2.2. Characterization of Er_2O_3 nanoparticles

The size and structure of the nanoparticles was studied by methods of X-ray diffraction (XRD) patterns. These were collected with a Rigaku Miniflex diffractometer coupled with a Cu source at 40 kV ($\lambda = 1.54056$ Å). The morphology of the nanoparticles was studied by confocal microscopy and atomic force microscopy (AFM). For the former, the images were recorded with a 3D confocal microscope ContourGT-K from Bruker. The magnification was set at 100X, with a vertical range of 500 nm. The AFM micrographs were recorded by an AFM easyScan 2 from Nanosurf. It had a high-resolution head of 10 μm with a standard silicon tip. The imaging mode was set at static-force (contact). On the other hand, the absorption spectra were recorded by an Ocean Optics QE65000 spectrometer and a deuterium-halogen lamp

as illumination source. A pulsed tunable MOPO-SL system from Spectra-Physics was utilized as excitation source to obtain the luminescence spectra. The emission light from the samples was dispersed with a SpectraPro 500-i spectrograph, from Acton-Research and the signals were monitored with a R7400U-01 PMT from Hamamatsu. All measurements were performed at room temperature.

3. Results and discussion

3.1. Size, structure and morphology of Er_2O_3 nanoparticles

Figure 1 shows the recorded XRD pattern of the Er_2O_3 nanoparticles, which is indexed as crystalline Er_2O_3 with cubic structure (JCPDF file 77-0777). No characteristic peaks of impurities were observed on the pattern. The size of the nanoparticles was calculated by the Scherrer's formula: $d = 0.9\lambda/\beta\cos\theta$, where λ is the X-ray excitation wavelength, θ is the Bragg angle and β is the experimental full width at half maximum for the strongest reflection peak (222) for Er_2O_3. The calculated size was about 32 nm.

Confocal microscopy and AFM were utilized to determine the morphology of the nanoparticles. Figure 2 shows an optical microscope image of the Er_2O_3 nanoparticles. The amplification was insufficient to estimate the size or shape. However, the micrograph suggests that most nanoparticles were agglomerated in clusters. On the other hand, AFM images were recorded in order to study the morphology of the samples with more detail, as shown on the micrograph of Fig. 3. The nanoparticles had spherical shape with a peak of the size distribution centered at 40 nm (not shown), as calculated by the Feret's diameter measured from AFM images.

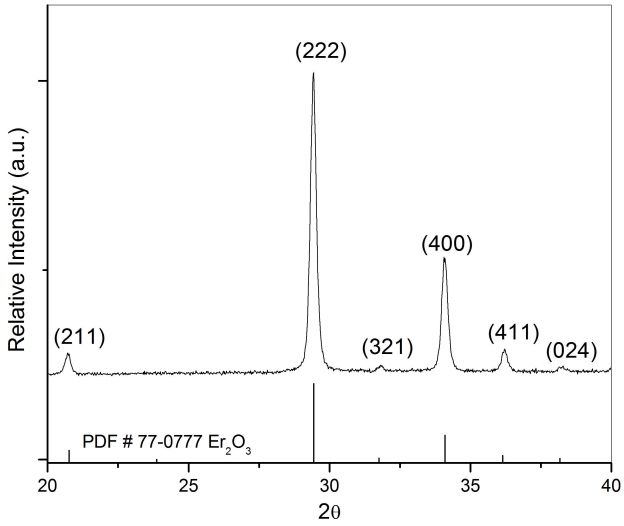

FIGURE 1. XRD pattern of the Er_2O_3 nanoparticles and the reference data of PDF # 77-0777 for pure Er_2O_3.

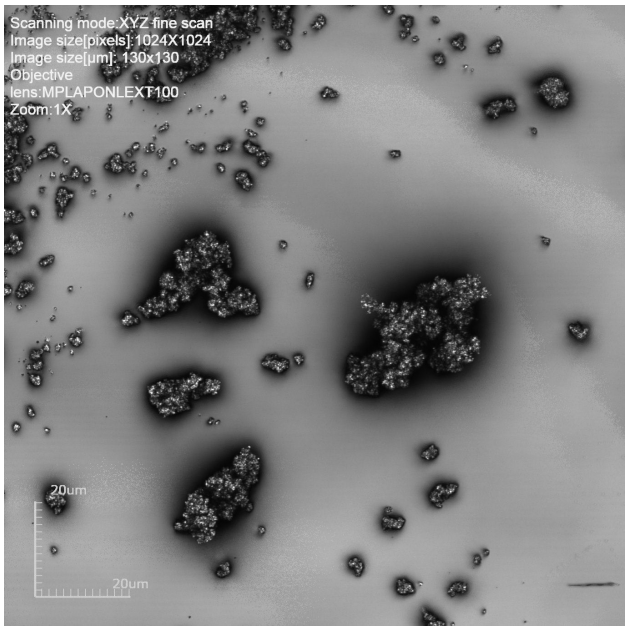

FIGURE 2. Confocal microscope image of Er_2O_3 nanoparticles.

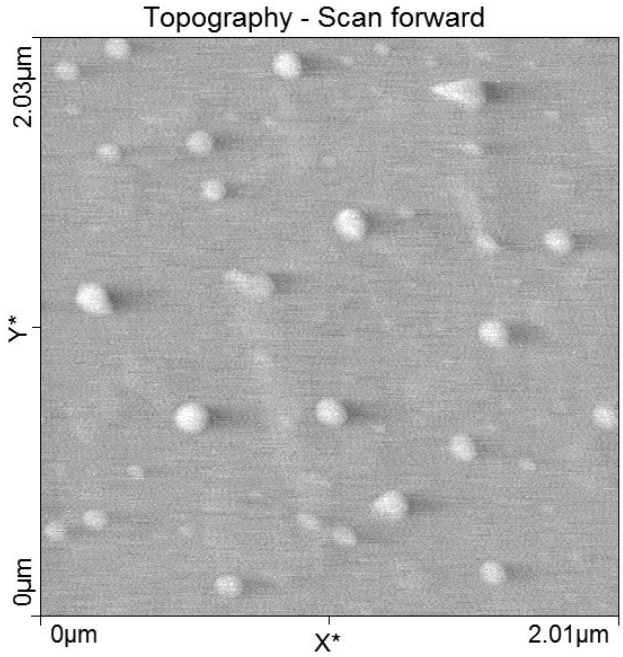

FIGURE 3. AFM micrograph of Er_2O_3 nanoparticles.

3.2. Optical characterization of Er_2O_3 nanoparticles

3.2.1. Absorption spectrum

Figure 4 shows the absorption spectrum of the Er_2O_3 nanoparticles within a wavelength range from 350 nm to 980 nm. The spectrum depicts characteristic absorption bands of erbium ions, and were identified as the Stark levels associated with the $^{2S+1}L_J$ manifolds of the electronic energy configuration of Er^{3+} [3].

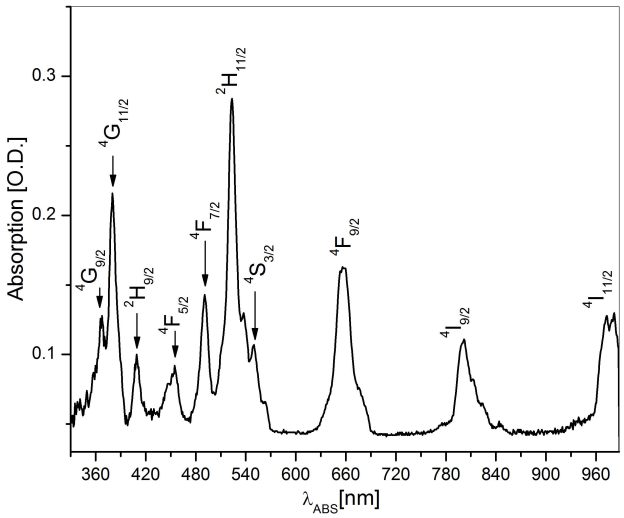

FIGURE 4. Absorption spectrum of the Er_2O_3 nanoparticles with the corresponding excited states of Er^{3+} ($4f^{11}$).

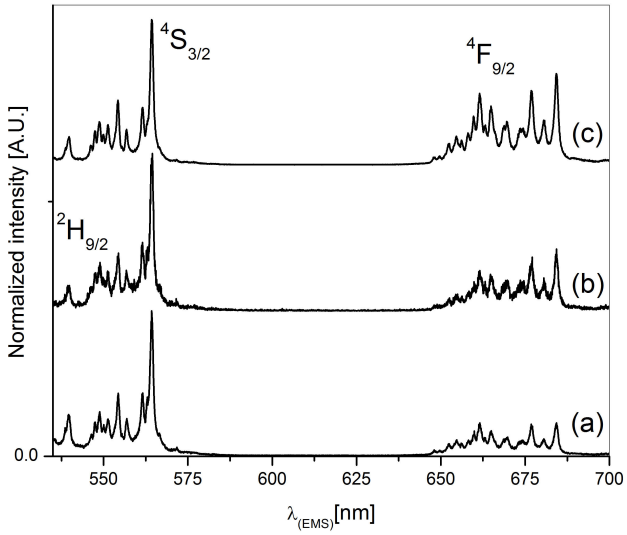

FIGURE 5. Luminescence spectra at room temperature from Er_2O_3 nanoparticles at different excitation wavelengths: (a) 525 nm, (b) 805 nm and (c) 975 nm.

TABLE I. Experimental energy levels and absorption energies of Er^{3+} in Er_2O_3

$^{2S+1}L_J{}^a$	λ(nm)^b	O.D.^{c}	E_{exp}(cm^{-1})^d
$^4I_{11/2}$	981	0.12	10190
	973	0.12	10271
$^4I_{9/2}$	811	0.08	12318
	800	0.11	12507
$^4F_{9/2}$	657	0.16	15202
	652	0.15	15337
$^4S_{3/2}$	549	0.1	18214
$^2H_{11/2}$	522	0.28	19157
$^4F_{7/2}$	490	0.14	20408
$^4F_{5/2}$	453	0.09	22052
$^2H_{9/2}$	409	0.1	24467
$^4G_{11/2}$	379	0.21	26385
$^4G_{9/2}$	366	0.12	27322

[a] Stark levels of Er^{3+} ($4f^{11}$).

[b] Peak of the Absorption wavelength.

[c] Optical Density (Peak values).

[d] Experimental energy of transitions.

Table I shows the analysis of the experimental energy levels related to the absorption spectrum of our samples. These results were in good agreement with the experimental values reported by Gruber *et al*. [21] for Er^{3+} in nanocrystalline Er_2O_3 and for Er^{3+}:Y_2O_3.

3.2.2. *Luminescence properties from Er_2O_3 nanoparticles*

Visible luminescence from Er^{3+} was obtained by pumping the Er_2O_3 nanoparticles at 525 nm, 805 nm and 975 nm. Figure 5 shows the recorded spectra within the wavelength range from 500 nm to 700 nm. These spectra are characteristic of Er^{3+} down conversion and upconversion. The stronger emission bands were centered at 560 nm and 680 nm and are attributed to radiative transitions $^4S_{3/2} \longrightarrow {}^4I_{15/2}$ and $^4F_{9/2} \longrightarrow {}^4I_{15/2}$, respectively [9]. The less intense emission band in the region of 510-530 nm is assigned to the transition $^2H_{11/2} \longrightarrow {}^4I_{15/2}$. The position of the luminescence peaks was similar for each excitation wavelength, although the red emission had different intensities. Table II shows the energies of the green and red emissions from Er_2O_3 irradiated at 975 nm. Our results show a good agreement with these reported by Chandra *et al* [22].

3.2.3. *Excitation mechanisms*

The simplified excited levels diagram of Er^{3+} on Fig. 6a shows direct excitation of Er^{3+} from the ground state to $^2H_{11/2}$ at 525 nm pump wavelength. From $^2H_{11/2}$ state, Er^{3+} underwent the radiative transition $^4I_{9/2} \longrightarrow {}^4I_{11/2}$, as well as multi-phonon relaxations to the lower lying excited states $^4S_{3/2}$ and $^4F_{9/2}$. Radiative decays from these states produced the depicted green and red emissions, which are reported so far [9].

It is well known that up-conversion is produced by mechanisms such as excited state absorption (ESA) and energy transfer (ET) processes. ESA process involve a single ion, and thus is often related to materials with low dopant content, while ET usually involves the interaction among two or more ions and depends on the dopant content [23]. Therefore, the most probable process in our samples was ET, because the high erbium content in Er_2O_3, as reported on [24]. This favours ET due to a reduction of the distance between Er^{3+} [25]. Figure 6b shows the proposed excitation paths of Er^{3+} irradiated at 805 nm. The absorption of 805 nm pump photons excited erbium ions from $^4I_{15/2}$ ground state to $^4I_{9/2}$ state. Subsequently, these ions interact through the ET process ($^4I_{9/2} + {}^4I_{9/2}$)$\longrightarrow$($^2H_{9/2}$, $^4I_{15/2}$), thereby enabling the

TABLE II. Experimental transition energies of Er^{3+} in Er_2O_3.

$^{2S+1}L_J$ [a]	λ(nm) [b]	O.D. [c]	Transition [d]	E_{Exp}(cm^{-1}) [e]
$^2H_{11/2}$	525.57	0.05	$T_3 \longrightarrow Z_3$	19026
	526.56	0.06	$T_3 \longrightarrow Z_4$	18991
	532.64	0.04	$T_1 \longrightarrow Z_6$	18774
	535.37	0.05	$T_4 \longrightarrow Z_8$	18678
	539.68	0.19	$T_1 \longrightarrow Z_8$	18529
$^4S_{3/2}$	546.35	0.13	$U_2 \longrightarrow Z_2$	18303
	547.31	0.23	$U_2 \longrightarrow Z_3$	18271
	548.88	0.30	$U_1 \longrightarrow Z_1$	18218
	549.87	0.21	$U_1 \longrightarrow Z_2$	18186
	551.45	0.27	$U_1 \longrightarrow Z_4$	18134
	554.18	0.44	$U_2 \longrightarrow Z_5$	18044
	556.91	0.24	$U_1 \longrightarrow Z_6$	17956
	561.61	0.40	$U_2 \longrightarrow Z_8$	17805
	564.17	1.00	$U_1 \longrightarrow Z_8$	17730
$^4F_{9/2}$	648.10	0.05	$V_5 \longrightarrow Z_1$	15429
	649.68	0.06	$V_5 \longrightarrow Z_2$	15392
	652.41	0.14	$V_4 \longrightarrow Z_1$	15327
	654.57	0.19	$V_5 \longrightarrow Z_5$	15286
	656.15	0.16	$V_4 \longrightarrow Z_4$	15240
	658.09	0.21	$V_3 \longrightarrow Z_4$	15195
	659.67	0.33	$V_4 \longrightarrow Z_5$	15159
	661.61	0.49	$V_3 \longrightarrow Z_5$	15114
	663.18	0.27	$V_4 \longrightarrow Z_6$	15078
	664.96	0.40	$V_2 \longrightarrow Z_5$	15038
	668.67	0.26	$V_5 \longrightarrow Z_7$	14955
	669.66	0.30	$V_5 \longrightarrow Z_8$	14932
	673.77	0.25	$V_4 \longrightarrow Z_7$	14841
	674.55	0.25	$V_4 \longrightarrow Z_8$	14824
	676.89	0.51	$V_3 \longrightarrow Z_8$	14773
	680.1	0.30	$V_2 \longrightarrow Z_8$	14703
	684.15	0.63	$V_1 \longrightarrow Z_8$	14616

[a] Stark levels of Er^{3+} ($4f^{11}$).

[b] Absorption wavelength.

[c] Optical Density.

[d] Radiative transitions from the Stark levels: T_n, U_n and V_n.

[e] Measured energy of transitions in Er^{3+} excited at 975 nm.

excitation of $^2H_{9/2}$ [26]. Figure 6b also shows the population of next lower states $^4F_{5/2}$, $^4F_{7/2}$ and $^4I_{11/2}-^4S_{3/2}$ by no-radiative decays, as on Ref. 27. Then the Er^{3+} gave the depicted green luminescence from these excited states [28].

The population paths of Er^{3+} pumped at 975 nm are shown on Fig. 6b. The first Er^{3+} excited state is $^4I_{11/2}$, whose lifetime is around 10 ms, as reported for an oxide-based matrix [29]. This lifetime enables the population of the manifold $^4I_{11/2}-^4S_{3/2}$ by the ET process $(^4I_{11/2} + {}^4I_{11/2}) \longrightarrow (^4S_{3/2} + {}^4I_{15/2})$.

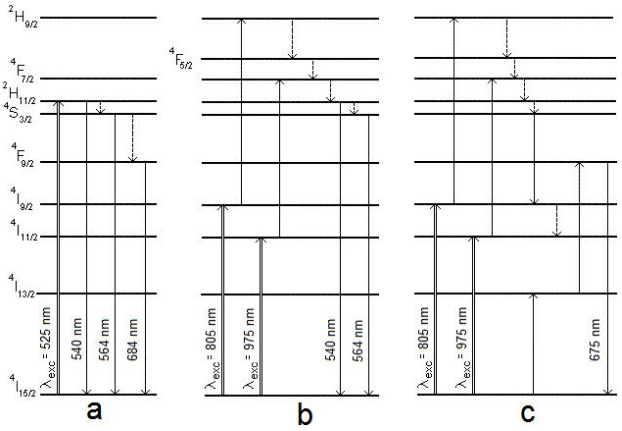

FIGURE 6. Simplified energy-levels diagram of Er^{3+} and the excitation paths proposed for: (a) the down conversion emission bands obtained with 525 nm excitation, (b) the green up conversion luminescence for 805 nm and 975 nm excitation wavelengths and (c) Excitation of $^4F_{9/2}$ state by pumping the Er_2O_3 nanoparticles at 805 nm and 975 nm.

3.2.4. Red up-conversion luminescence ($^4F_{9/2} \longrightarrow {}^4I_{15/2}$)

Figure 6c shows the proposed excitation paths for $^4F_{9/2}$ state when Er^{3+} is irradiated at 805 nm and 975 nm. Subsequent no-radiative decays populated $^4S_{3/2}$ state, which is related with the population of $^4F_{9/2}$. The corresponding excitation mechanism are described on [23], where an erbium ion reaches the $^4I_{13/2}$ state by the cross relaxation $(^4S_{3/2},\ {}^4I_{15/2}) \longrightarrow (^4I_{9/2}, {}^4I_{13/2})$. Subsequently, the interaction among excited erbium ions through ET $(^4I_{13/2}, {}^4I_{11/2}) \longrightarrow (^4F_{9/2},\ {}^4I_{15/2})$ leaves an Er^{3+} in the ground state and the other in the excited state $^4F_{9/2}$.

The spectra depicted on Fig. 5 show a variation of the red to green emission ratio upon the wavelength excitation. The trend of the integrated areas from the luminescence spectra is shown on Fig. 7, where the smallest red area corresponded to the excitation at 525 nm. This is expected as the non-radiative transition $^4S_{3/2} \longrightarrow {}^4F_{9/2}$ involves the emission of several phonons to bridge the energy gap between $^4S_{3/2}$ and $^4F_{9/2}$ states, which limits the red emission at some extent. The depicted rise of the red areas for 805 nm and 975 nm pump wavelengths may be explained in terms of the oscillator strength f, or equivalently, the transition probabilities, where a value of $f \sim 1$ represents a strong transition, while a forbidden transition might have $f \sim 09$ [30]. The oscillator strength is calculated by the following expression [31]:

$$f = \frac{1}{108.9cl} \int O.D.\lambda(\lambda) d\lambda,$$

where C is the concentration of the Er^{3+} (mol/L), l is the path length (cm) and $O.D.$ is the optical density in wavenumbers. The calculated oscillator strength for the transition $^4F_{15/2} \longrightarrow {}^4I_{11/2}$, was $f = 0.40$; whereas a value of $f = 0.12$ was obtained for $^4I_{15/2} \longrightarrow {}^4I_{9/2}$. A similar trend is found in the literature [32,33]. These results suggest an increase for the red emission from the former transition as a

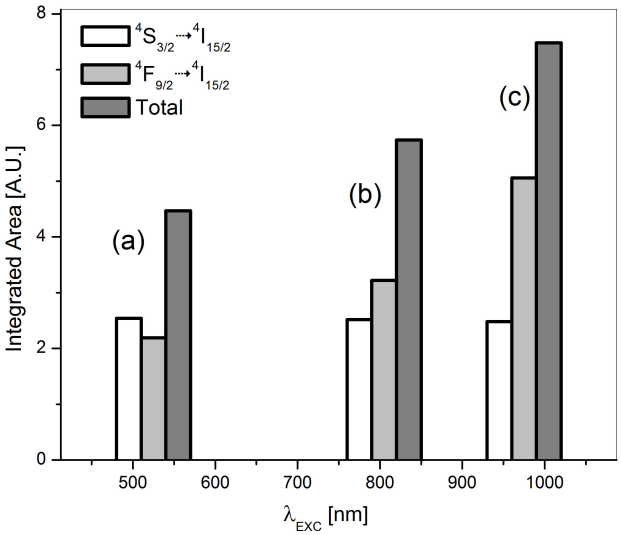

FIGURE 7. 7 Integrated luminescence from Er_2O_3 nanoparticles pumped at: (a) 525nm, (b) 805 nm, and (c) 975 nm.

larger amount of erbium ions could reach the $^4S_{3/2}$ state by pumping at 975 nm, in comparison to these excited at 805 nm.

The latter are in agreement with the cross sections reported elsewhere for the involved transitions: the absorption cross section for $^4I_{15/2} \longrightarrow {}^4I_{11/2}$ has a value of 3.2; whereas the value reported for the transition $^4I_{15/2} \longrightarrow {}^4I_{9/2}$ is 1.7 for glasses doped with Er_2O_3 [34]. Cross sections, not calculated here, quantify the ability of an ion to absorb and emit light. There are several works that report this parameter with similar values in different hosts, which support our assumptions regarding the effect of the different pumping schemes on the red emission.

4. Conclusions

We report the synthesis, structural and optical characterization of Er_2O_3 nanoparticles stabilized with ascorbate ligands. The recorded spectra shown intense and sharp luminescence peaks for the green ($^4S_{3/2} \longrightarrow {}^4I_{15/2}$) and red ($^4F_{9/2} \longrightarrow {}^4I_{15/2}$) emission bands centered at about 560 nm and 680 nm, respectively. An enhancement of the red emission was recorded for up-conversion luminescence. This was due to the influence of the phonon-assisted population mechanisms and to the transition rates of Er^{3+}.

1. K. Binnemans, *Chem. Rev.* **109** (2009) 4283
2. L. Maia, A. Ibanez, L. Ortega, V. Mastelaro, A.C. Hernandes, *J. Nanopart. Res.* **10** (2008) 1251.
3. A. Kenyon, *Progress in Quantum Electronics* **26** (2002) 225.
4. A. Bahtat, M. Marco de Lucas, B. Jacquier, B. Varvel, M. Bouazoui, J. Mugnier, *Opt. Mater* **7** (1997) 173
5. J. García, R. Plugaru, B. Méndez, J. Piqueras, T. Tate, *Eur. Phys. J. Appl. Phys.* **27** (2004) 75.
6. Q. Xiang, Y. Zhou, B.S. Ooi, Y.L. Lam , Y.C. Chan, C.H. Kam *Thin Solid Films* **370** (2000) 243.
7. L. Zamperdi, M. Ferrari, C. Armellini, F. Visintainer, C. Tosello, S. Ronchin, *J. Sol-Gel. Sci. Technol.* **26** (2003) 1033.
8. Z. Pan, S.H. Morgan, A. Loper, V. King, B.H. Long, and W.E. Collins, *J Appl Phys.* **77** (1995) 4688.
9. F. Auzel, *Chem. Rev.* **104** (2004) 139
10. E. Castagna *et al*., *Mater. Sci. Eng. B* **105** (2003) 83.
11. A. Sobolev, *Microelect. J.* **26** (1995) 725
12. E. Chryssou, W. Pitt, *J. of Quantum elect. IEEE* **72** (2008) 282.
13. M. Grishin, I. Khartsev, O. Dzibrou *J. Appl. Phys.* **105** (2009) 113.
14. Z. Chen *et al*., *J. Am. Chem. Soc.* **130** (2008) 3023.
15. L. Fuh, *Thin Solid Films* **518** (2010) 5044.
16. V. Sudarsan, S. Sivakumar, F.C. van Veggel, *Chem. Mater*. **17** (2005) 4736.
17. R. Diamente, C. van Veggel, *J. Fluoresc*. **15** (2005) 543.
18. K. Lunstroot, L. Baeten, P. Nockemann, J. Martens, P. Verlooy, X. Ye, *J. Phys. Chem. C* **113** (2009) 13532.
19. S. Sivakumar, F. van Veggel, M. Raudsepp, *J. Am. Chem. Soc.* **127** (2005) 12464.
20. S. Sivakumar, F. van Veggel, M. Raudsepp, *Journal of the American Chemical Society* **127** (2005) 12464.
21. J. Gruber, J. Burdick, S. Chandra, D. Sardar, *Journal of Applied Physics* **108** (2010) 23109.
22. S. Chandra, F. Deepak, J. Gruber, D. Sardar *J. Phys. Chem. C.* **114** (2010) 874.
23. J. Castañeda, M. Meneses, O. Barbosa, R. Chiu, M. Félix, and R. Rodríguez, *J. of Lumin* **130** (2010) 2356.
24. R. Aghamalyan *et al*., *J. of Contemporary Phys.* **44** (2009) 291.
25. C. Yeh, A. Shibley, I. Schneider, S. Afzal, I. Aggarwal, *J. of Appl. Phys*. **69** (1991) 1684.
26. P. Hehlen, J. Cockroft, and R. Gosnell, *Phys. Rev. B* **56** (1997) 9302.
27. A. Capobianco, F. Vetrone, C. Boyer, A. Speghini, M. Bettinelly, *J. Phys. Chem. B* **106** (2002) 1181.
28. J. Castañeda, M. Meneses, O. Barbosa, E. de la Rosa, F. Mosiño, *J of Lumin.* **102** (2003) 504.
29. C. Becker, A. Olsson, R. Simpson, *Erbium-Doped Fiber Amplifiers: Fundamentals and Technology*, (Academic Press, USA, 1999).
30. M. Hubert, J. Sandeman, *Rep. Prog. Phys.* **49** (1986) 397.
31. K. Binnemans, L. Jongen, W.C. Gorller, *Phys. Chem. Chem. Phys.* **3** (2001) 4796.
32. Q. Nie, L. Lu, T. Xu, S. Dai, X. Shen, X. Liang, X. Zhang *Journal of Physics and Chemistry of Solids* **67** (2006) 2345.
33. L. Hai, G. Meredith, S. Jiang, X. Peng, T. Luo, N. Peyghambarian, P. Yue, *Appl. Phys.* **93** (2003) 186.
34. Y. Choi, K. Kim, *J. Am. Ceram. Soc.*, **82** (1999) 2762.